Journal of Inorganic Biochemistry 145 (2015) 1–10

Contents lists available at ScienceDirect

Journal of Inorganic Biochemistry

journal homepage: www.elsevier.com/locate/jinorgbio

Synthetic, potentiometric and spectroscopic studies of chelation between Fe(III) and 2,5-DHBA supports salicylate-mode of siderophore binding interactions

Suheel K. Porwal [a], Emilia Furia [b], Michael E. Harris [c], Rajesh Viswanathan [d,*], L. Devireddy [a,**]

[a] Case Comprehensive Cancer Center and Department of Pathology, Case Western Reserve University, Cleveland, OH 44106, USA
[b] Department of Chemistry and Chemical Technologies, University of Calabria, Arcavacata di Rende, 87036 CS, Italy
[c] Department of Biochemistry, Case Western Reserve University, Cleveland, OH 44106, USA
[d] Department of Chemistry, Case Western Reserve University, Cleveland, OH 44106, USA

ARTICLE INFO

Article history:
Received 5 June 2014
Received in revised form 5 December 2014
Accepted 6 December 2014
Available online 15 December 2014

Keywords:
2,5-DHBA
Gentisic acid
Iron chelation
Salicylate mode
UV–Vis spectroscopy

ABSTRACT

Catecholate type enterobactin, a prototype siderophore, comprises 2,3-dihydroxybenzoic acid (2,3-DHBA) cyclically linked to serine in *E. coli*. The existence of iron-chelating ligands in humans is a recent discovery, however, the basic chemical interactions between 2,5-dihydroxybenzoic acid and Fe(III) ion remain poorly understood. Achieving an accurate description of the fundamental Fe(III) binding properties of 2,5-DHBA is essential for understanding its role in iron transport mechanisms. Here, we show that 2,5-DHBA binds iron in a salicylate mode via a two-step kinetic mechanism by UV spectroscopy. Complexation between Fe(III) salt and 2,5-DHBA initially occurs at 1:1 ratio (of ligand to metal) and binding resulting in higher-order complexes continues at higher concentrations. Through potentiometric measurements we quantify the distribution of Fe(III)-2,5-DHBA complexes with 1:1, 1:2 and 1:3 stoichiometry. The formation of 1:3 complexes is further supported through high-resolution mass spectrometry. Further, using kinetic and equilibrium UV spectroscopy, we report Fe(III)-2,5-DHBA complex formation at a pH range of 2.5–9.0 at 298.15 K in water. Maximum complexation occurred at a pH range of 4.5–6.5 consistent with deprotonation of the carboxylic acid proton. Equilibrium measurements and stopped-flow kinetics show that complexation rate constants were independent of concentrations of 2,5-DHBA. Together the data supports a model in which the rate-determining step involves rearrangement of ligands on an initial complex formed by reversible binding between the carboxylate group of 2,5-DHBA and Fe(III).

1. Introduction

Recent discoveries reveal the existence of low-molecular weight iron-binding compounds in eukaryotic cells that are capable of mediating iron transportation [1–7]. It was recently reported that 2,5-dihydroxybenzoic acid (gentisic acid) is a key iron-chelating moiety in eukaryotic cells [7]. Indeed, there is a remarkable conservation of the biosynthetic pathways for 2,5-DHBA production in eukaryotes and 2,3-dihydroxybenzoic acid, which is the iron-binding moiety of *E. coli* siderophore enterobactin [8]. In *E. coli*, enterobactin is biosynthesized in a series of reactions catalyzed by at least six enzymes [9]. Among these enzymes, 2,3-dihydro-2,3-dihydroxybenzoate dehydrogenase (EntA) catalyzes the rate-limiting production of 2,3-dihydroxybenzoate in enterobactin biosynthesis. Significantly, we identified an EntA homologue in eukaryotes, BDH2, another member of the short chain dehydrogenase family responsible for 2,5-DHBA biosynthesis [7]. As with enterobactin, any functional eukaryotic siderophore probably contains additional molecules besides 2,5-DHBA. Nonetheless, 2,5-DHBA alone is sufficient to chelate and transport iron into the mitochondria [7,10].

While the biological role of 2,5-DHBA is an area of intense interest [6,7,11,12], the basic chemical interactions between 2,5-DHBA and Fe(III) ion that are essential for understanding its biological function remain poorly understood. For example, despite evidence for its in vivo function, recent biochemical analyses showed surprisingly low apparent affinity of 2,5-DHBA for Fe(III), and attempts to co-crystallize 2,5-DHBA and Fe(III) bound to lipocalin were unsuccessful [13]. Molecular modeling suggests that the salicylate mode of binding assumed for 2,5-DHBA, in which a carboxyl and an adjacent hydroxyl group on the siderophore interact simultaneously with the bound metal, is incompatible with binding to lipocalin 24p3 [13].

The fact that 2,5-DHBA could effectively transport Fe(III) across the cell in eukaryotes [7] presented an apparent paradox in light of the studies published recently [13] and warranted a reasonable explanation for the binding modes displayed by 2,5-DHBA. Therefore, we examined more closely the complexation reaction of 2,5-DHBA and Fe(III) using

* Corresponding author. Tel.: +1 216 368 3696; fax: +1 216 368 3006.
** Corresponding author. Tel.: +1 216 368 1513; fax: +1 216 368 0494.
E-mail addresses: rajesh.viswanathan@case.edu (R. Viswanathan), lxd59@case.edu (L. Devireddy).

http://dx.doi.org/10.1016/j.jinorgbio.2014.12.010
0162-0134/

potentiometric measurements, mass spectrometry, and equilibrium and kinetic UV spectroscopy to characterize the structure and stability of the complexes formed and the mechanism of binding. The data reported here unambiguously demonstrate rapid complexation between Fe(III) salts and 2,5-DHBA through a salicylate mode of binding with multiple 2,5-DHBA ligands interacting with a single Fe(III) metal center. We attribute the appearance of new peaks observed using UV spectroscopy due to formation of Fe(III) complexes, and present further evidence to support this notion through potentiometric analyses and mass spectrometry. The final states of the complexes engage multiple stoichiometry involving 2,5-DHBA as ligands and are likely to involve a 1:3 complex **3**. We also document slow changes in UV absorbance that were consistent with breakdown of the 2,5-DHBA potentially via oxidation involving the hydroxyl group at the 5 position. The long term instability of the complexes observed here would thus explain the inability of previous studies to detect their formation. These data are important in establishing the ability of 2,5-DHBA to complex with Fe(III) ion in vitro and providing a rationale for apparently conflicting biochemical observations regarding 2,5-DHBA complexation properties.

2. Experimental

2.1. Synthesis of Fe(III)-2,5-DHBA complex

2.1.1. Method A

2,5-DHBA (230.0 mg, 1.49 mmol) dissolved in ethanol (4.0 mL) was added to a premixed ethanolic solution of NaOH (60.0 mg, 1.49 mmol in 2.0 mL of EtOH) under constant stirring. Next, $Fe(NO_3)_3 \cdot 9H_2O$ (200.0 mg, 0.50 mmol in 1.0 mL EtOH) was slowly added at room temperature over a period of 20 min. The reaction mixture was vortexed for 30 min to maintain homogeneity of the solution. The complexation over 12 h resulted in precipitation of $NaNO_3$, which was removed by filtration. The resulting solution was evaporated to give a dark blue-colored solid, which was estimated to be 62% of input (158 mg, 0.30 mmol). The solid was analyzed by mass spectrometry after solubilizing in DMSO. The mixture was also analyzed by UV–visible (UV–Vis) spectroscopy after diluting with water.

2.1.2. Method B

2,5-DHBA (342.0 mg, 2.22 mmol) in methanol (10.0 mL) was added to a premixed ethanolic solution of NaOH (89.0 mg, 2.22 mmol in 2.0 mL EtOH) under constant stirring. Next, $FeCl_3 \cdot 6H_2O$ (200.0 mg, 0.74 mmol in 1.0 mL MeOH) was slowly added at room temperature over a period of 30 min. The reaction mixture was stirred for an additional 12 h at room temperature to complete the complexation. Upon complexation, a dark blue-colored mixture was obtained, which was filtered using a Whatman filter. The resulting dark blue-colored complex was estimated to be 66% of input (251.0 mg, 0.49 mmol). The mixture was then analyzed by UV–Vis spectroscopy after diluting with water. The solid was next analyzed by mass spectrometry after solubilizing in DMSO.

2.2. Equilibrium and kinetic UV–Vis spectroscopy of Fe(III) complexes

UV–Vis spectra, in scanning mode, were obtained on a Shimadzu UV-1800 spectrophotometer, which was equipped with a TCC-240A thermoelectrically controlled cell holder (Shimadzu). Data were obtained as absorbance values and were analyzed in Microsoft excel® and Origin®. The time dependent change in absorbance due to chelation was monitored using stopped flow spectroscopy using an Applied Photophysics pi*-180 spectrometer, at fixed wavelength. Solutions of 100–600 μM $FeCl_3 \cdot 6H_2O$ and 2,5-DHBA were mixed using the instruments stopped flow unit with a total shot volume of 150 μL and a flow cell with a 1 cm path length at 298.15 K. The absorbance at 590 nm (2 nm slit width) was collected in 100–400 points over 1–10 s. The rate constants for individual kinetic traces were determined by fitting to a single exponential function. Fits to this equation gave essentially random residuals and averages of >3 individual kinetic traces provided estimates of experimental error of ca. 10%.

2.3. Speciation study using potentiometry

A perchloric acid stock solution was prepared and standardized as described previously [14]. A sodium perchlorate stock solution was prepared and standardized according to Biedermann [15]. Sodium hydroxide titrant solutions were prepared and standardized as described previously [16]. Fe(III) perchlorate was prepared and standardized as reported by Ciavatta et al. [17]. All carbonate free solutions were prepared under inert atmosphere with double distilled water. The cell arrangement was similar to that described by Forsling et al. [18]. Ag/AgCl electrodes were prepared according to Brown [19]. Glass electrodes, manufactured by Metrohm, were of the 6.0133.100 type. They acquired a constant potential within 10 min after the addition of the reagents and remained unchanged within ± 0.1 mV for several hours. The titrations were carried out with a programmable computer controlled data acquisition switch unit 34970 A supplied by Hewlett Packard. The electro motive force (EMF) values were measured with a precision of $\pm 10^{-5}$ V using an OPA 111 low-noise precision DIFET operational amplifier. A slow stream of nitrogen gas was passed through four bottles (a–d) containing: a) 0.96 mol kg^{-1} NaOH, b) 0.94 mol kg^{-1} H_2SO_4, c) twice distilled water, and d) 1.05 mol kg^{-1} $NaClO_4$, and then into the test solutions, stirred during titrations, through the gas inlet tube. During the EMF measurements, the cell assembly was placed in a thermostat kept at (298.15 ± 0.1) K.

2.4. Mass spectrometry

MS analyses were performed on a Thermo Scientific LTQ-FT™ (a hybrid mass spectrometer consisting of a linear ion trap, low resolution) and/or a Fourier transform ion cyclotron resonance mass spectrometer (FT-ICR, TOF-ESMS).

3. Results and discussion

3.1. Synthesis and stability of Fe(III)-2,5-DHBA complex

As shown in Fig. 1, depending on the acid dissociation constant (pK_a), one or multiple protons of 2,5-DHBA may be lost to give rise to a bidentate ligand binding ion (in its salicylate mode) with the possibility of any of the three complexes (**1**, **2** or **3**) as a result of complexation [14]. The pK_a of the three acidic protons in 2,5-DHBA are reported at 3.1 (COOH), 10.46 (C2 phenoxyl) and 13.41 (C5 phenoxyl) respectively [20]. In a simplistic model, without considering stereochemical isomerism, the complexes **1**, **2** and **3** could in principle co-exist at equilibrium, once Fe(III)-salt (e.g. $FeCl_3.6H_2O$ or $Fe(NO_3)_3.9H_2O$) and 2,5-DHBA are complexed in aqueous solution. Through systematic variation of ligand-to-metal stoichiometry, we designed conditions to enable the generation of Fe(III)-2,5-DHBA complexes. The relative populations of each individual complex were expected to be a function of stoichiometry of Fe(III) and 2,5-DHBA. Synthetic methods that were employed for populating the 3:1 complex **3** are shown in Scheme 1. 2,5-DHBA was treated with sodium hydroxide in ethanol as a solvent (in which 2,5-DHBA dissolves completely) to generate the carboxylate ion of 2,5-DHBA. Ferric chloride hexahydrate was pre-dissolved in ethanol and this solution was titrated slowly into the carboxylate salt solution of 2,5-DHBA.

After addition of the aqueous solution of $FeCl_3 \cdot 6H_2O$ to a 2,5-DHBA or 5-MeO-SA solution, a drastic color change was noticed due to the ligand to metal charge transfer and the solution turned from colorless to deep blue instantaneously. When compared to the existing literature on Fe(III) complexes of comparable ligands, the observed color change seems reasonable and expected [21]. After filtration, we obtained a dark blue amorphous solid indicating the formation of

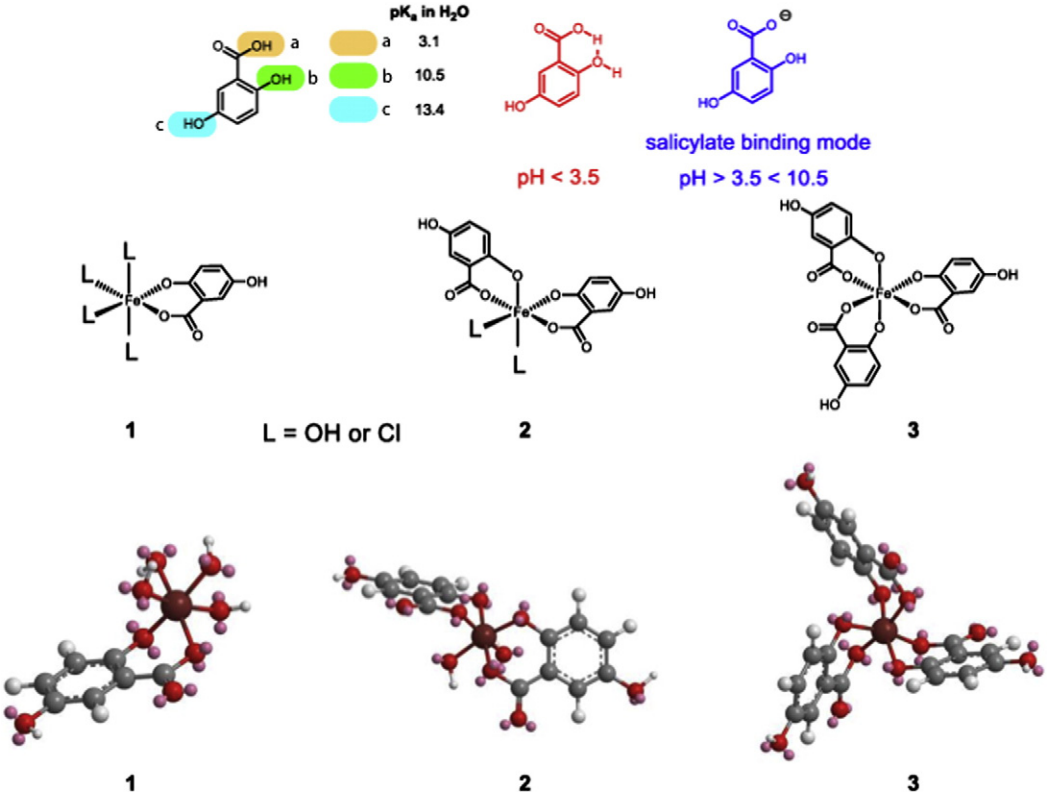

Fig. 1. Top: 2,5-DHBA or gentisic acid. The three acidic positions are shown in color. The protonated form and the mono anion are shown in red and blue respectively. Bottom: Structures of Fe(III)-2,5-DHBA complexes with a 1:1 (**1**), 2:1 (**2**) and a 3:1 (**3**) ratio of 2,5-DHBA:Fe(III) ion. Structures are Chem3D depictions with L = OH or Cl ions.

a complex (Scheme 1). This complexation reaction was reproducible and the change in color was consistent and predictable over several attempts. The complex formed through the synthetic method involving $FeCl_3 \cdot 6H_2O$ was used for analyses (by UV–Vis spectroscopy as described in Section 3.2 and via mass spectrometry as shown in Section 3.4). The alternative method employed for the formation of complexes involved reaction of the carboxylate salt of 2,5-DHBA and $Fe(NO_3)_3 \cdot 9H_2O$. In this reaction the by-product, sodium nitrate

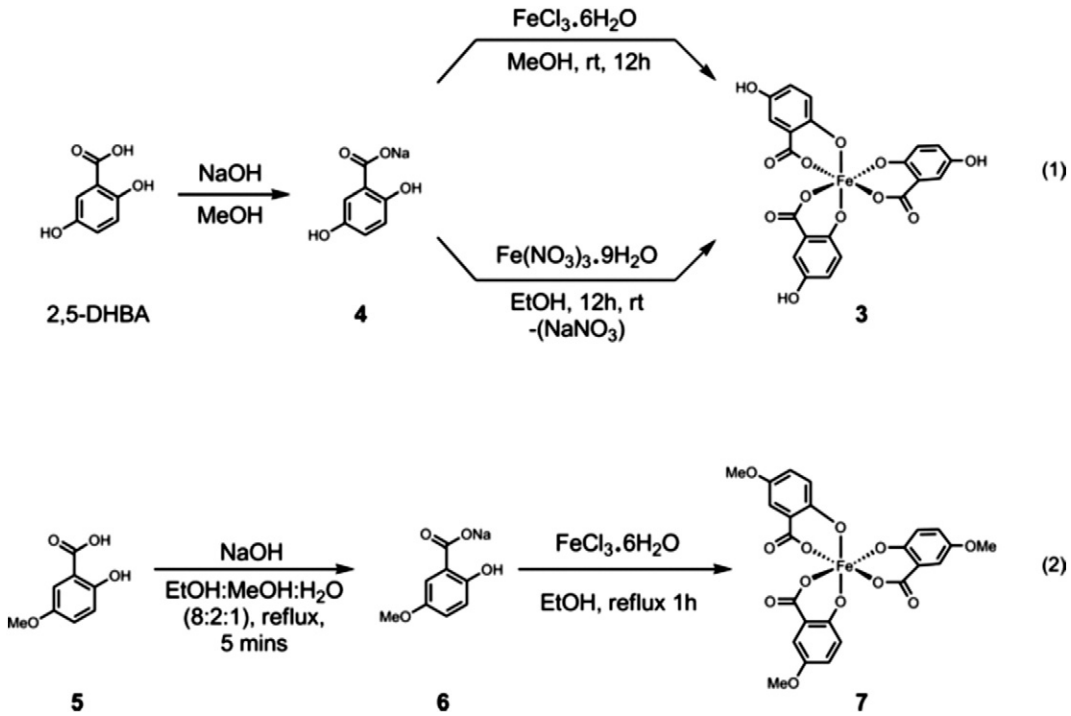

Scheme 1. Synthesis of complexes **3** and **7**. Equation 1 shows the formation of complex **3** from 2,5-DHBA. Two distinct conditions were employed involving $FeCl_3 \cdot 6H_2O$ and $Fe(NO_3)_3 \cdot 9H_2O$. Complex **7** is formed from its corresponding carboxylate salt upon binding with $FeCl_3 \cdot 6H_2O$.

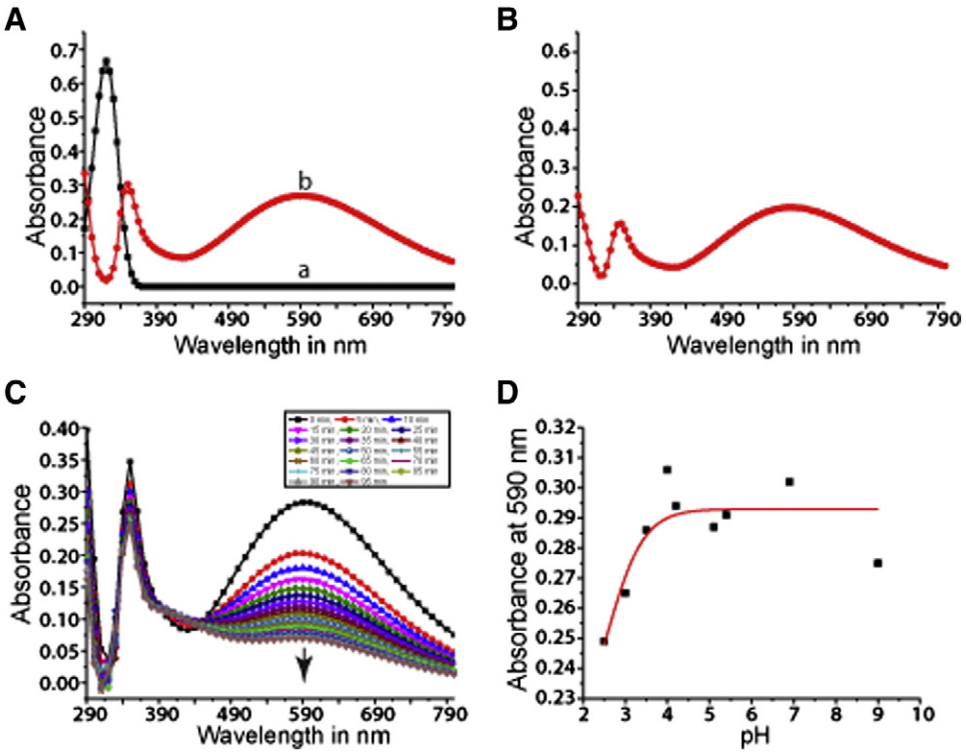

Fig. 2. A. UV–Vis spectrum of 162 μM 2,5-DHBA in water at pH 6.4 (black, line a); and the complex formed between 648 μM 2,5-DHBA and 216 μM $FeCl_3 \cdot 6H_2O$ in water at pH 6.4 (red, line b). B. UV–Vis spectrum of 149 μM 5-MeO-SA in water at pH 6.8 (black); and complex formed between 297 μM 5-MeO-SA and 99 μM $FeCl_3 \cdot 6H_2O$ in water at pH 6.8 (red). C. UV–Vis plot of absorbance versus wavelength for the complex formation between 648 μM 2,5-DHBA and 216 μM $FeCl_3 \cdot 6H_2O$ in water at pH 6.4 at 5 minute intervals (from 0 to 95 min). The arrow indicates direction of absorbance change with time. D. Plot of absorbance (at 590 nm) as a function of pH (range = 2.5 to 9.0) showing existence of 590 nm peak indicative of Fe(III)-2,5-DHBA complex **3**. Plot is fit to a model for a single activating deprotonation. The equation for the fit is: y = A + (B / (1 + 10^(K − x))) where A = initial absorbance, B = maximum absorbance, K = the pKa value of the functional group undergoing deprotonation. The apparent pKa is 2.56 ± 0.799; A = 0.21 ± 0.08 and B = 0.08 ± 0.8. $R^2 = 0.626$. pH in each titer was controlled (to the specific value as displayed) prior to complexation through pre-formation of the carboxylate ion of 2,5-DHBA as shown in Scheme 1.

precipitated out and was filtered off to result in an amorphous solid complex **3**. Because of the presence of a chromophore in 2,5-DHBA, we conducted extensive analyses of this complex-forming reaction using UV–Vis spectroscopy (Fig. 2A). UV–Vis studies were performed on complexes formed through the reaction of 2,5-DHBA and $FeCl_3 \cdot 6H_2O$ (Scheme 1, equation 1, top) while HR-MS studies were performed on complexes formed through the reaction of 2,5-DHBA and $Fe(NO_3)_3 \cdot 9H_2O$ (Scheme 1, equation 1, bottom). Yields of complex **3** formation using these two methods were 62% and 66% respectively (Table 1).

In order to test the salicylate-binding mode between 2,5-DHBA and Fe(III) ion, we used 5-methoxysalicylic acid (5-MeO-SA), a surrogate of 2,5-DHBA that cannot bind through the methylated oxygen to Fe(III) ion. Upon complexation, 5-MeO-SA provided similar UV–Vis spectroscopic results to those observed earlier for 2,5-DHBA (complex **3**), indicating the formation of Fe(III)-5-MeO-SA complex **7** (Fig. 2A & B).

Table 1
Isolated percent yields of complexes **3**, **7**, **8** and **9** from synthetic methods employed as shown in Schemes 1 and 2.

Entry	Complex	Structure	Yield (%)
1.	$Fe^{(III)}$-$(2,5\text{-DHBA})_3$	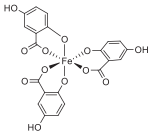	62 (with $Fe(NO_3)_3 \cdot 9H_2O$ 66 (with $FeCl_3 \cdot 6H_2O$)
2.	$Fe^{(III)}$-$(5\text{-MeO-SA})_3$	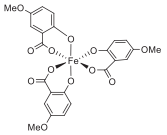	61
3.	$Cr^{(III)}$-2,5-DHBA$(en)_2$	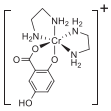	78
4.	$Fe^{(III)}$-2,5-DHBA$(en)_2$	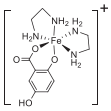	54

As shown in equation 2 in Scheme 1, we observed complexation of 5-MeO-SA to $FeCl_3 \cdot 6H_2O$ under refluxing conditions in ethanol to result in complex **7** in 61% isolated yield (Table 1). Sodium salt of 5-MeO-SA displayed poor solubility in ethanol, and therefore a mixture of ethanol, methanol and water in the ratio of 8:2:1 (respectively) was employed. The color change observed during the formation of 2,5-DHBA complex **3** was observed in this case as well. The solutions containing complexes **3** and **7** were analyzed individually by UV–Vis spectroscopy (Figs. 2, 3 and 4) and mass spectrometry (Table 3).

Analogously, we prepared complexes of Fe(III)-2,5-DHBA and Cr(III)-2,5-DHBA, in the presence of ethylenediamine to serve as stable bidentate ligand to enhance formation of stable complexes **8** and **9** respectively. Therefore, chromium(III) chloride hexahydrate was mixed with 2,5-DHBA and ethylenediamine in the presence of zinc dust as a reducing agent in methanol under refluxing conditions over 2 h as shown in equation 3 (Scheme 2). The ensuing complex **8** was isolated in 78% yield using procedures similar to the Fe(III)-2,5-DHBA complex **3** (Table 1). Similar to the complexation described for the chromium(III) ion, Fe(III) was subjected to complexation in the presence of ethylenediamine ligand and zinc dust in hot methanol over 2 h. The stable complex **9** depicted in equation 4 was obtained in 54% isolated yield (Table 1).

3.2. Equilibrium and kinetic UV-Vis spectroscopy of Fe(III)-2,5-DHBA complexation

Initially, we attempted several methods (i.e. layering, vapor diffusion and slow evaporation) for crystallization of Fe(III)-2,5-DHBA complex but unfortunately failed to get diffraction quality crystals for X-ray analysis. While crystallographic data would provide strong corroborative structural evidence, considering this failure of the complex to crystallize and considering the fact that there are UV–Vis reports for benzoic acid-like ligands chelated to Fe(III), we turned to generating equilibrium and kinetic UV–Vis data in the hope that it can be interpreted in terms of a consistent and chemically accurate binding model.

Therefore, we compared the UV spectra of the free and bound 2,5-DHBA, and analyzed the time dependent changes in UV absorbance during complexation (Figs. S1–S3). 2,5-DHBA has a strong absorption in the UV–Vis range of electromagnetic spectrum (λ_{max} at 320 nm; $\varepsilon = 3700\ M^{-1}\ cm^{-1}$; Fig. S2). Upon addition of $FeCl_3 \cdot 6H_2O$ to 2,5-DHBA in solution (1:3 ratio of Fe(III) salt:2,5-DHBA) the UV–Vis data showed a 30 nm bathochromic (red) shift in absorbance (of the corresponding peak for 2,5-DHBA) indicating that there was complexation occurring (Fig. 2A). The color change that occurred was also observed during synthesis of this complex and was concomitant with release of

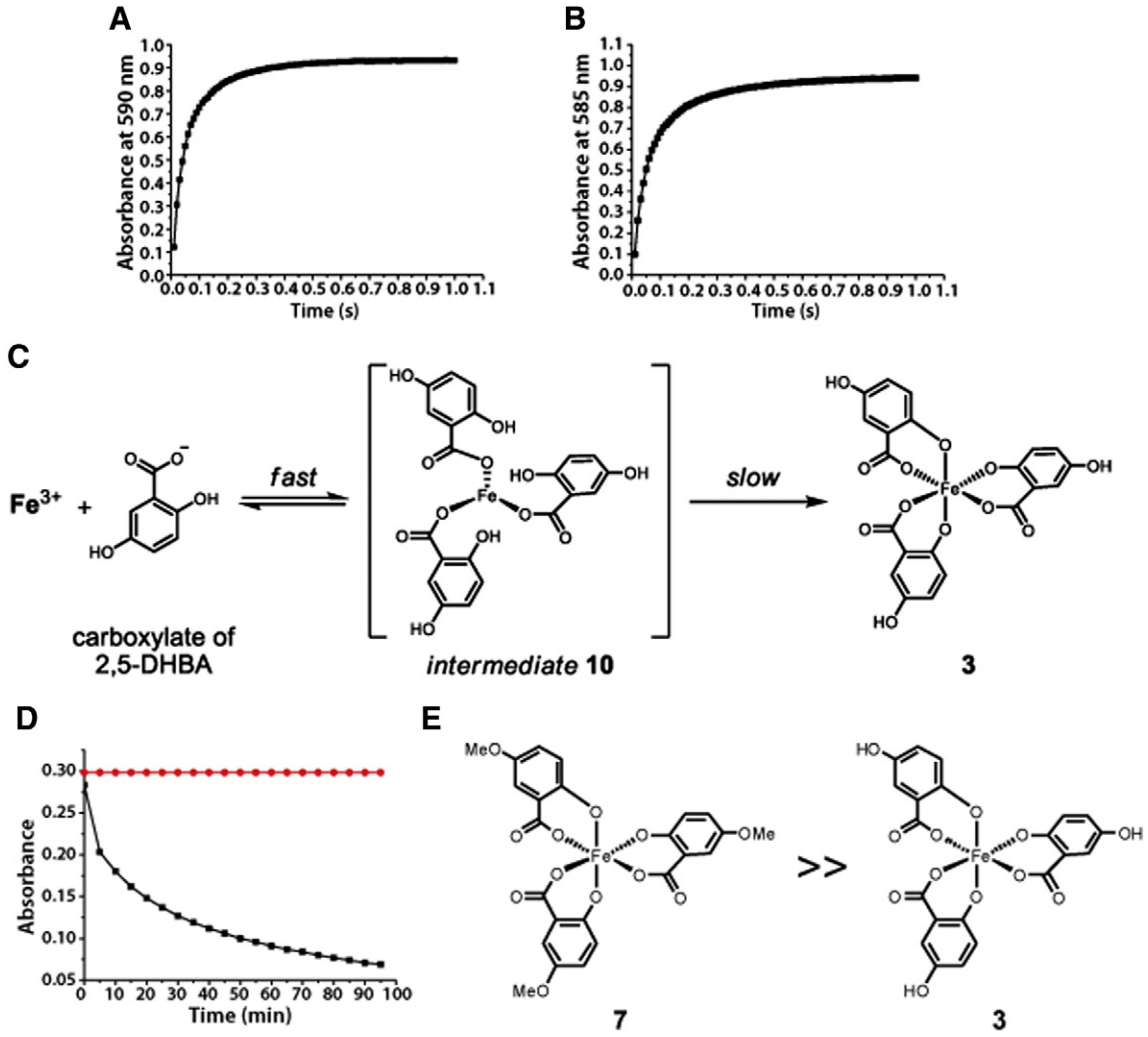

Fig. 3. Kinetic plots of Fe(III)-2,5-DHBA binding followed through stopped-flow UV spectroscopy. A. Plot of absorbance (at 590 nm) versus time (s) measured for complex formation between 2,5-DHBA (648 μM) and $FeCl_3 \cdot 6H_2O$ (216 μM) in water at pH 6.4. B. Plot of absorbance (at 582 nm) versus time (s) measured for complex formation between 5-MeO-SA (594 μM) and $FeCl_3 \cdot 6H_2O$ (198 μM) in water at pH 6.8. C. Fast and slow complexation events in the formation of complex **3**. D. Comparative time dependent study for measuring the stability of the complex formed between 445 μM 5-MeO-SA and 148 μM $FeCl_3 \cdot 6H_2O$ at pH 6.8 (red, absorbance at 582 nm, the near horizontal line at the upper part) and 648 μM 2,5-DHBA and 216 μM $FeCl_3 \cdot 6H_2O$ at pH 6.4 (black, absorbance at 590 nm) with 5 min intervals. E. Comparable stability of complexes **3** and **7**.

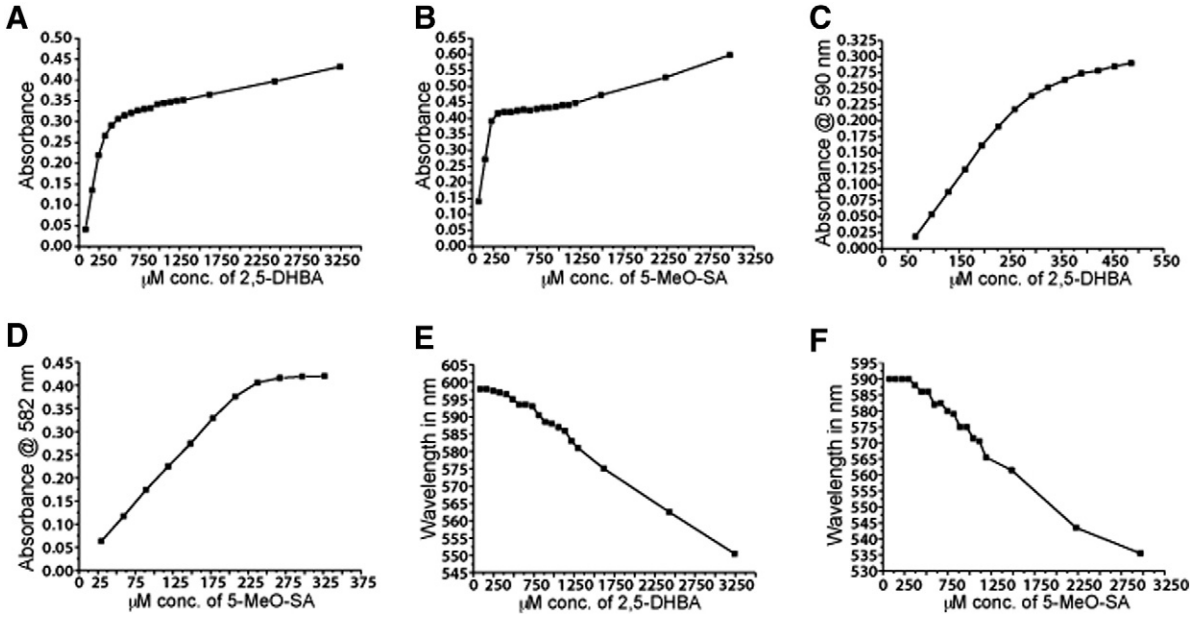

Fig. 4. A. UV–Vis spectra of $FeCl_3.6H_2O$ (220 μM) with varying concentration of 2,5-DHBA in water at pH 6.4 at 298.15 K; B. UV–Vis spectra of $FeCl_3.6H_2O$ (220 μM) with varying concentration of 5-MeO-SA in water at pH 6.8 at 298.15 K; C. UV–Vis spectra of the titration between $FeCl_3.6H_2O$ (220 μM) and varying concentration of 2,5-DHBA in water at pH 6.4 at 298.15 K. D. UV–Vis spectra of the titration between $FeCl_3.6H_2O$ (207 μM) and varying concentration of 5-MeO-SA in water at pH 6.5 at 298.15 K; E. UV–Vis spectra of the titration between $FeCl_3.6H_2O$ (220 μM) and 2,5-DHBA in water defined as λ_{max} as a function of conc. of 2,5-DHBA at pH 6.4 at 298.15 K; F. UV–Vis spectra of the titration between $FeCl_3.6H_2O$ (220 μM) and 2,5-DHBA in water defined as λ_{max} as a function of conc. of 5-MeO-SA at pH 6.8 at 298.15 K.

nitrate from $Fe(NO_3)_3 \cdot 9H_2O$. Scanning between 290 and 800 nm revealed two new peaks for the complex at $\lambda_{max} = 350$ nm and at 590 nm (a ligand-to-metal charge transfer band) respectively. We attribute these new peaks as a result of formation of Fe(III) complexes, as indicated by potentiometric analyses and mass spectrometry the final state is likely to be complex **3**. The shoulder observed at 320 nm for the mixture is due to the small amount of unbound 2,5-DHBA. Furthermore, high-spin Fe(III) has no spin-allowed d–d transitions. Therefore we attribute the UV–Vis spectra of Fe(III)-2,5-DHBA chelate complex **3** to arise from the coulombic interaction between the positively charged metal ion and the negatively charged oxygen atoms through a charge-transfer transition.

In addition to the rapid initial changes in UV absorbance we also observe a time-dependent decrease of the intensity of the ligand to metal charge transfer band at 590 nm, while the peak at 350 nm retained its intensity over time (Fig. 2C). The d^5 electronic configuration of Fe^{3+} rules out any crystal field stabilization energy (CFSE) and makes the complexes relatively labile with respect to isomerization and ligand exchange in aqueous solution. The UV spectral data indicate that formation of the complex is rapid, but that a second process, potentially

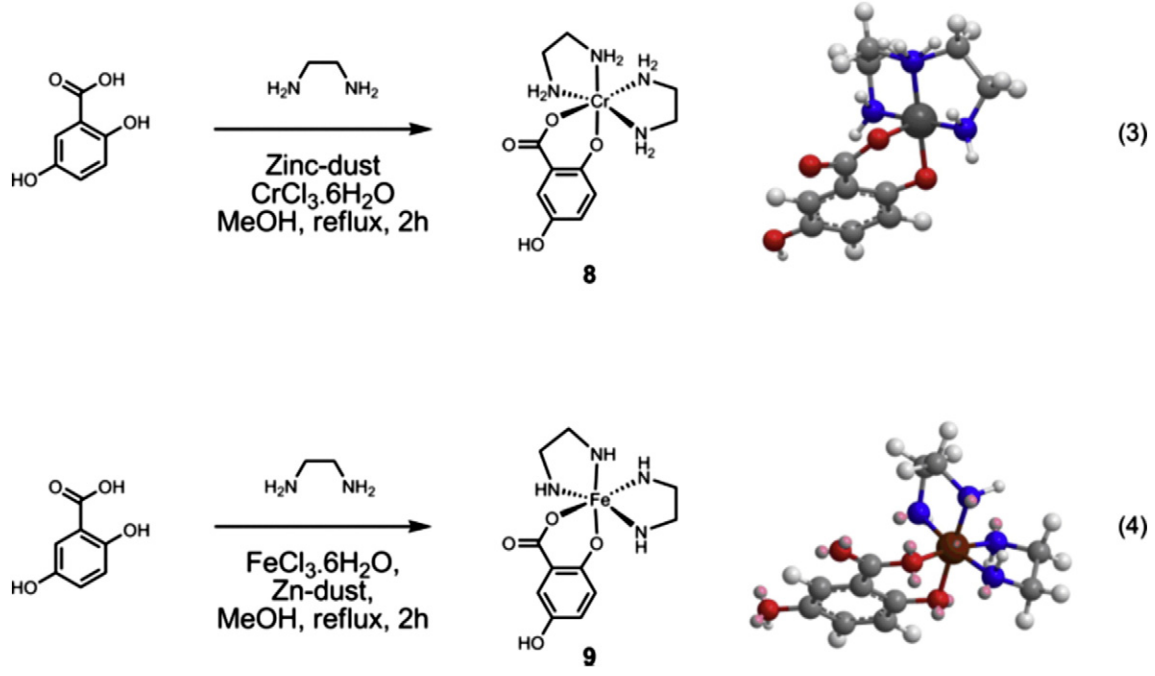

Scheme 2. Synthesis of Cr(III) and Fe(III) complexes (**8** and **9**) with 2,5-DHBA and supporting ethylenediamine ligands.

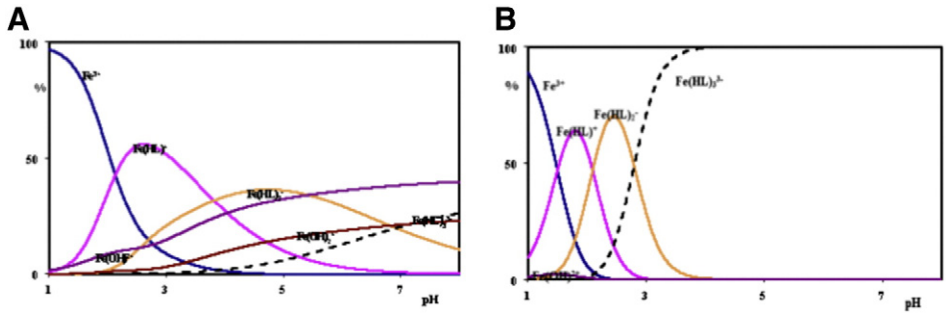

Fig. 5. Distribution of the Fe(III) species, expressed as percentages (%) versus pH, in: (A) $C_L = 1$ mM, $C_M = 1$ mM; (B) $C_L = 9.7$ mM, $C_M = 1$ mM. The percentage of total Fe in the different protonated and liganded forms (Fe^{3+}; $Fe(HL)^{+}$; $Fe(HL)_2^{-}$; $Fe(HL)_3^{3-}$; $Fe(OH)^{2+}$ and $Fe(OH)_2^{+}$) are shown as a function of pH. For clarity a dotted line is used for $Fe(HL)_3^{3-}$.

oxidation of the 2,5-DHBA, occurs at a slower time scale. Nevertheless, these results in conjunction with speciation distribution shown in Fig. 5 are consistent with the interpretation that the rate of complexation out competes hydrolysis of the complex until further oxidation of complex **3** occurs. In order to further validate 2,5-DHBA as a chelating bidentate ligand to metals, a kinetically more inert d^3 center of Cr^{3+} was complexed with 2,5-DHBA resulting in complex **8**. Because Cr^{3+} metal center possesses similar ionic radii and the same charge as Fe(III), complex **8** demonstrates a high degree of structural similarity to complex **3**. As observed through mass spectrometry, the binding of 2,5-DHBA to Cr(III) was evident further confirming that the ligand is capable of binding to metals through a salicylate mode. The extinction coefficient of 2,5-DHBA in Fig. 2A (black) and for 5-MeO-SA in Fig. 2B (black) are 4111 and 5900 M^{-1} cm^{-1} respectively. Whereas the apparent extinction coefficient for the complex Fe(III)(2,5-DHBA)$_3$ (**3**) in Fig. 2A and for Fe(III)(5-MeO-SA)$_3$ in Fig. 2B are 460 and 666 M^{-1} cm^{-1} respectively.

To better understand the mechanism of complex formation and factors that influence its stability, we analyzed the pH dependence of complex formation and the kinetics of the complexation reaction using stopped flow UV spectroscopy. The increase in absorbance at 350 nm and 590 nm due to complexation occurs rapidly, within the mixing time of the experiment (1–2 min). The pH dependence of complex formation between 2,5-DHBA and Fe(III) as monitored by UV spectroscopy is shown in Fig. 2D. As described above, if the binding reaction requires deprotonation of one or more of the titratable protons on 2,5-DHBA, then there will be an increase in bound Fe(III) dependent on the pK_a of the titratable group. One of the two signature bands, namely the 590 nm band, assigned to the formation of Fe(III)-2,5-DHBA complex **3**, was monitored as a function of varying pH from 2.5 to 9.0 (Fig. 2D). The R^2 fit of 0.626 in Fig. 2D, is not very good is due to the complexes' being labile on a longer time scale. These data fit a mechanism involving deprotonation of a single functional group necessary for complex formation yielding an estimated pK_a of 3.1, which presumably reflects the carboxyl group. Given the proximity of the carboxylic acid and the hydroxyl at the 2 position, the most likely mode of binding of Fe(III) involves the carboxylic acid and the adjacent hydroxyl (salicylate mode).

Stopped flow UV spectroscopic data presented in Fig. 3A show that mixing of 648 μM 2,5-DHBA and 216 μM $FeCl_3 \cdot 6H_2O$ results in a rapid increase in absorbance at 590 nm in a single phase with an apparent rate constant of *ca.* 10 s^{-1}. This result is consistent with the rapid change in the spectrum of 486 μM 2,5-DHBA upon mixing with 162 μM $FeCl_3 \cdot 6H_2O$ as shown in SI (Fig. S7). An essentially identical kinetic profile is seen for the binding reaction containing 5-methoxy derivative of 2,5-DHBA and Fe(III) ion (Fig. 3B). The presence of the methyl group at the 5 position should preclude this moiety from serving as a metal ion coordination ligand. Thus, the increase in 590 nm absorbance is clearly attributable to the formation of Fe(III)-2,5-DHBA complex and the simplest model for the binding, which is consistent with the available biochemical and biophysical data, is the salicylate mode involving the carboxylic acid and the hydroxyl group at the 2 position.

Interestingly, variation of 2,5-DHBA and Fe(III) over a ~10-fold concentration range did not result in any significant change in the observed rate constant (Fig. S7). Because of the intermolecular nature of the reaction, association is necessarily sensitive to concentration. Thus, the complexation event monitored by the increase in absorbance most likely reflects a process occurring subsequent to initial intermolecular association. As shown in Fig. 3C, a simple model is that initial association occurs via the carboxyl group, which is followed by coordination of the proximal hydroxyl group resulting in the charge transfer band and absorbance at 590 nm. Regarding the mechanism presented in Fig. 3C no assumptions were made regarding the loss of bound water from the metal ion, though it was considered a possibility. However, for loss of water from the metal ion to be overall rate limiting, then the re-association of water would have to be much slower than association with 2,5-DHBA, which is unlikely given the differences in concentration (55 M versus ca. 300 μM). However, the equilibrium between fully hydrated and partially dehydrated Fe could limit the concentration of "active" Fe that is available for complexation. In this case a concentration dependence of the reaction would still be expected. The limiting concentration of dehydrated Fe would simply limit the magnitude of the second order association rate constant without resulting in concentration independent behavior. Regardless, the data shows that the bimolecular association step (*fast*) is not rate limiting for complex formation, and that the general mechanism in Fig. 3C is the most plausible mechanism involving a relatively *slow* reorganization of the ligand on intermediate **10**.

Data in Fig. 3D show that the absorbance corresponding to the ligand-to-metal charge transfer band at 590 nm steadily decreases over *ca.* 100 min when 2,5-DHBA is the ligand whereas the corresponding methyl substituted complex **7** maintained high absorbance at 582 nm. Importantly, stopped flow experiments showed the same kinetics for complex formation, but lacked the second slower phases observed for 2,5-DHBA. These results are significant for two reasons. First, they demonstrate that complex formation is not dependent on coordination to the hydroxyl at the 5 position of the aromatic ring. Second, they indicate that the slower decrease in absorbance is not relevant to complex formation and likely involves chemical decomposition involving this functional group. We hypothesize that in the case of 2,5-DHBA, the formation of single electron oxidative transformations (leading to quinone forms) may cause the decrease in absorbance, which will not occur in the case of the methyl derivative. Relative stability therefore follows the order shown in Fig. 3E.

Next, we used the change in UV absorbance upon 2,5-DHBA binding to examine the stoichiometry of complex formation. In an equilibrium binding reaction, if the concentration of 2,5-DHBA or 5-MeO-SA is above the K_d for Fe(III) binding, then the concentration dependence of the UV signal will be linear until the stoichiometric concentration of the ligand is reached. At that point there will be no additional increase in absorbance associated with binding due to stoichiometric titration of the Fe(III) by 2,5-DHBA or 5-MeO-SA. The range of the ligand

concentration in this titration varied between 1:5 (ligand:Fe(III)) to a >10:1 (ligand:Fe(III)). The results (as illustrated in Fig. 4A and B) clearly show two linear phases in the titration data, a linear increase followed by lack of concentration dependence. The inflection point (~300 μM for 2,5-DHBA, Fig. 4A) indicates the concentration of the ligand necessary to bind all of Fe(III) in the assay. Similarly, the inflection point (~250 μM for 5-MeO-SA, Fig. 4B) indicates the concentration of the ligand necessary to bind all of Fe(III) in the assay. The simple interpretation to explain this data is that a 1:1 complex forms that results in the absorbance change. Fig. 4C and D illustrate this binding event by illustrating the concentration range from 50 to 500 μM for 2,5-DHBA and 25 to 350 μM for 5-MeO-SA, respectively. This experiment supports a model in which 2,5-DHBA or 5-MeO-SA can form a 1:1 complex, but does not provide information on whether a 1:2 or 1:3 complex can subsequently form when additional 2,5-DHBA or 5-MeOSA is added at constant metal concentration.

UV–Vis data of the titration experiments demonstrate that a 1:1 complex between Fe(III) and 2,5-DHBA are formed initially at equivalent concentrations at 590 nm (298.15 K) above the dissociation constant, however, additional multimers form at higher concentrations as indicated by the gradual and steady increase in absorbance (Fig. 4A and B). An accompanying gradual shift in the λ_{max} (wavelength) is plotted as a function of concentration of ligands in Fig. 4E and F respectively for 2,5-DHBA and 5-MeO-SA. As observed for all Fe(III)-ligand complexes reported in this study, the peak at ~590 nm is attributed to the ligand-to-metal charge transfer process. Furthermore, the existence of additional multimers at higher ligand to metal stoichiometry is supported by potentiometric titration experiments.

3.3. Speciation study spanning pH 1–8 through potentiometric analysis

A sensitive means to gain information on the formation and stoichiometry of metal complexes is potentiometric analysis, which measures, relative to a reference, the proportional change in solution potential due to changes in concentration of charged species. The complexation equilibria between Fe(III) and ligand were studied, at 298.15 K and in 1.05 mol kg^{-1} $NaClO_4$, by measuring with a glass electrode the competition of the 2,5-DHBA (H_3L) for the Fe(III) and H^+ ions. The metal and the ligand concentrations, C_M and C_L, respectively, ranged from (1–10 mM) and the ligand-to-metal ratio varied between 1 and 10. The hydrogen ion concentration varied from 10 mM (pH 2) to incipient precipitation of basic salts which takes place in the range $[H^+] = 0.1$–0.01 mM (pH 4–6) depending on the specific ligand-to-metal ratio. The general equilibrium can be written, schematically, as follows:

$$p\,Fe^{3+} + r\,H_3L \rightleftarrows Fe_pH_{-q}(H_3L)_r^{(3p-q)} + q\,H^+ \quad \beta_{pqr} \tag{2}$$

that takes into account the formation of simple ($q = r$), mixed ($q \neq r$), mononuclear ($p = 1$) and polynuclear ($p > 1$) species. The most probable p, q, and *r-values* and the corresponding constants β_{pqr} were calculated with least squares fitting of the potentiometric measurements [22]. In the numerical treatments the equilibrium constant concerning the species formed according to equilibrium (3) has been maintained invariant:

$$H_3L \rightleftarrows H_2L^- + H^+ \qquad \log\beta_1 = -2.61 \pm 0.02 \tag{3}$$

The first acidic constant of 2,5-DHBA, according to equilibrium 3, was determined by potentiometric measurements in the same experimental conditions used for the determination of stability constants between metal and ligand ions (i.e. at 298.15 K and in 1.05 M $NaClO_4$). The equilibrium constants for $FeOH^{2+}$, $Fe(OH)_2^+$ and $Fe_2(OH)_2^{4+}$ were fixed because they are well known from the literature [23,24]. The results for fitting these data to three models of increasing complexity are reported in Table 2.

Table 2
Best set of log β_{pqr} (σ) for the system 2,5-DHBA–Fe^{3+}, according to general equilibrium $p\,Fe^{3+} + r\,H_3L \rightleftarrows Fe_pH_{-q}(H_3L)_r^{(3p-q)} + q\,H^+$.

(pqr)	Model 1	Model 2	Model 3
$(1,2,1)^+$	-1.7 ± 0.1	-1.0 ± 0.1	-1.0 ± 0.1
$(1,4,2)^-$		-3.25 ± 0.08	-3.12 ± 0.04
$(1,6,3)^{3-}$			-6.6 ± 0.1
σ	0.968	0.416	0.251
χ^2	15.97	6.37	8.20
U	25.32	4.503	1.576

First, we assumed the presence of only $Fe(HL)^+$ (Model 1) but the standard deviation is higher than the experimental uncertainty. Additional models were tested by adding multiple liganded species; the better agreement was obtained with a model including complex $Fe(HL)_2^-$ (Model 2) with a consequent decrease of the function U equal to 82%. An additional improvement was reached including in the previous model the species $Fe(HL)_3^{3-}$ (Model 3). As no other species lowered the minimum, Model 3 was assumed as the best describing the data, also in consideration that the standard deviation (σ) is comparable with the experimental uncertainty. The refined equilibrium constants concerning the complexation of 2,5-DHBA with the Fe^{3+} ion, determined by potentiometric methods, are used to represent the distribution of the metal in the different species (Fig. 5).

As can be seen from Fig. 5, all the proposed complexes of types **1**, **2** and **3** in their protonated states are formed in appreciable amounts, particularly when the concentrations of ligand and metal are relatively high. In addition to mononuclear hydrated complexes, the deprotonated complexes $FeOH^{2+}$ and $Fe(OH)_2^+$ are also populated (Fig. 5A). When the concentration of ligand is greater than that of the metal $Fe(HL)^+$, $Fe(HL)_2^-$ and $Fe(HL)_3^{3-}$ reach significant percentages and predominate over the hydrolysis product. Significantly, the species with a stoichiometry of ligand to metal identical to complex **3** is the dominant species present at higher ligand ratios (Fig. 5B) confirming the model that 2,5-DHBA forms stable complexes with Fe(III) and showing that the formation of complex **3** at neutral pH is a process that still out competes the hydrolysis of complex **3**.

3.4. Mass spectrometric analysis of Fe(III)-2,5-DHBA complexes

In order to confirm the stoichiometry of 2,5-DHBA ligand to Fe(III) in the complexes we synthesized, we employed high resolution-mass spectrometry (HR-MS). The reduced solubility of complexes **3** and **7** in organic solvents limited their analysis to polar aprotic solvents. For example, complex **3** was found to be reasonably soluble only in DMSO or DMF for analyses by MS. Using electrospray ionization time of flight MS (ESI(+)-TOF-MS) analysis under positive ion mode, we confirmed the presence of complex **3** (Table 3, entry 1). The mass spectrum revealed the presence of three units of 2,5-DHBA to one unit of Fe(III) ion. The monoisotopic molecular ion ($M^+ = 518.0148$) as well as the isotopomer distribution of the M + 1 (519.0179) and M + 2 (520.0190) ions matched the expected masses for complex **3** (Fig. S8).

Complex **3** is only sparingly soluble in organic solvents but showed considerable solubility in DMSO, which was subsequently used as the solvent for sample ionization. By virtue of its nucleophilicity it displaced 2,5-DHBA ligands from complex **3** resulting in Fe(III)-2,5-DHBA–DMSO complexes of three distinct entities as shown by MS studies summarized in Table 3 (entries 2–4 and Figs. S9–12). One of the three complexes detected by HR-MS involved DMSO chelation to Fe(III) containing three ligands from DMSO and one unit of 2,5-DHBA (entry 2, m/z 441.9870).

The second complex had a m/z of 518.0000 and was assigned to a complex with two 2,5-DHBA and two DMSO units chelated to Fe(III) ion, as shown in entry 3. The third complex (entry 4, m/z 363.9733) was assigned a structure containing two DMSO and one 2,5-DHBA.

Table 3
High resolution mass spectrometry (HRMS) data showing presence of respective Fe(III)-2,5-DHBA and Cr(III)-2,5-DHBA complexes. Spectra shown in Fig. S8 for entry1; Fig. S10 for entry 2; Fig. S11 for entry 3; Fig. S12 for entry 4; Fig. S15 for entry 5; and Fig. S13 for entry 6.

Entry	Complex	Structure	Formula	HR-MS	
				Expected	Observed
1.	$Fe^{(III)}$-(2,5-DHBA)$_3$	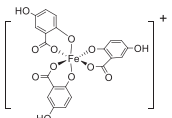	$[C_{21}H_{18}O_{12}Fe]^+$	518.0862	518.0148
2.	$Fe^{(III)}$-2,5-DHBA(DMSO)$_3$	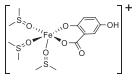	$[C_{13}H_{22}O_7S_3Fe]^+$	441.98716	441.98700
3.	$Fe^{(III)}$-(2,5-DHBA)$_2$(DMSO)$_2$	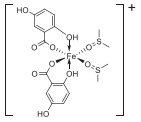	$[C_{18}H_{22}O_{10}S_2Fe]^+$	517.99983	518.00003
4.	$Fe^{(III)}$-2,5-DHBA(DMSO)$_2$	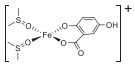	$[C_{11}H_{16}O_6S_2Fe]^+$	363.97322	363.97327
5.	$Fe^{(III)}$-(5-MeO-SA)$_2$	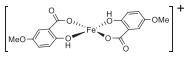	$[C_{16}H_{14}O_8Fe]^+$	390.00326	390.00352
6.	$Cr^{(III)}$-2,5-DHBA(en)$_2$	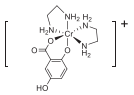	$[C_{11}H_{20}N_4O_4Cr]^+$	324.08842	324.08849

HRMS studies also revealed the presence of Fe(III) complexes conforming to the stoichiometry of Fe:L_2 and (Fe:L_2)$_2$ where L = 5-MeO-SA. MS peak at 390.0035 indicates the presence of Fe:L_2 complex and the peak at 778.9995 indicates the presence of (Fe:L_2)$_2$ (Figs. S14–16). HR-MS analyses confirmed the presence of complex **8** (Table 3, entry 6 and see Fig. S13). Overall, these studies are consistent with modeling and potentiometry data indicating complexation via multiple 2,5-DHBA groups in mononuclear complexes interacting via carboxylate chelation to the Fe(III) together with an interaction with the adjacent hydroxyl group at the 2 position (salicylate mode).

4. Discussion

Mitochondria are central to the regulation of cellular iron metabolism and the majority of iron imported into the cell is utilized within this organelle [1,4,7,12]. Unfortunately, little is known about the chaperones that facilitate intracellular iron trafficking [5]. We recently provided evidence supporting a role for 2,5-DHBA as a small molecule that binds and potentially trafficks iron into mitochondria [7]. However, understanding the biological role of 2,5-DHBA necessarily requires an accurate and complete description of the biochemical mechanism that mediates Fe(III) binding. Recent literature showed little apparent complex formation between 2,5-DHBA (gentisic acid) and Fe(III) ion relative to 2,3-DHBA, and intriguingly conflicted with an earlier report documenting the binding of 2,5-DHBA to Fe(III) [25,26]. Considering the established biological role of 2,5-DHBA as a facilitator of mitochondrial iron import [7], we attempted to clarify the underlying chemical factors that may contribute or encourage or limit binding between Fe(III) ion. Overall, the synthesis of Fe(III)-2,5-DHBA complexes led to characterization efforts through UV, potentiometry and mass spectrometry. Potentiometric titrations unambiguously identified binding constants and speciation between various forms of Fe(III) bound ligand complexes involving 2,5-DHBA. Additionally, the kinetics and pH dependence of binding using equilibrium and kinetic UV/Vis spectroscopy, illustrate the complex stoichiometry existing in solution. We acknowledge that limitations imposed by the relative instability of the complex make a conclusive interpretation of the identity of complexes difficult. In this report, we studied the complex formation of Fe(III)-salts with 2,5-DHBA in pH ranges of 2.5–9.0 at 298.15 K in water as solvent using kinetic and equilibrium UV spectroscopy, and confirmed the resulting structural complex through mass spectrometry. We observed that the maximum complexation occurred at pH 4.5–6.5 after the deprotonation of carboxylic acid proton. Through potentiometric measurements we quantitated the distribution of complexes with different stoichiometries and observed that a 10:1 ratio of ligand to metal strongly favors the presence of a species with three 2,5-DHBA ligands per Fe(III) nucleus, which was confirmed by high-resolution mass spectrometry. Through equilibrium measurements and stopped-flow kinetics we report that complexation rate constants are independent of concentrations of 2,5-DHBA indicating that a slow step involves rearrangement of a pre-formed complex preceded by a fast and reversible binding step involving the carboxylate group and Fe(III) ion. Based on the results presented here, we propose a model involving a complexation of 2,5-DHBA that binds to Fe(III) in a salicylate mode of binding. While 2,5-DHBA, or its modified counterparts have been studied as a bidentate ligand to lanthanides [27] and other metals [28–34], there is limited data relevant to binding to Fe(III) in the literature [35]. The model presented here represents an important advance because it provides a chemical basis for understanding the biological activity shown by 2,5-DHBA in the context of a postulated mammalian siderophore. It is to be noted that a microbial siderophore (like enterobactin) is transported across the membrane by a cognate receptor protein recognizing a specific siderophore, however; no such outer membrane receptors are reported for Fe(III)-2,5-DHBA complexes. It is possible that some complex of Fe(III)-[2,5-DHBA]$_3$ could transport Fe(III) across a eukaryotic cell membrane.

Acknowledgments

We thank Robert B. Petersen for editorial assistance. This work is supported by grants from NIH (K01CA113838 and R01DK081395), American Cancer Society (RSG1328901TBE) and Case Western Reserve University start up funds to L.R.D. L.R.D. is also a recipient of career developmental awards from March of Dimes and American Society of Hematology.

Appendix A. Supplementary data

General experimental information on methods for the synthesis of complexes **7**, **8** and **9**, additional UV–Vis plots and copies of mass spectrometry data for complexes **3**, **7**, **8** and **9** are provided. Supplementary data to this article can be found online at http://dx.doi.org/10.1016/j.jinorgbio.2014.12.010.

References

[1] J.B. Neilands, J. Biol. Chem. 270 (1995) 26723–26726.
[2] R.C. Hider, X. Kong, Nat. Prod. Rep. 27 (2010) 637–657.
[3] R.C. Hider, X. Kong, Dalton Trans. 42 (2013) 3220–3229.
[4] M. Miethke, M.A. Marahiel, Microbiol. Mol. Biol. Rev. 71 (2007) 413–451.
[5] J.A. Fernandez-pol, Biochem. Biophys. Res. Commun. 78 (1977) 136–143.
[6] Z. Liu, R. Lanford, S. Mueller, G.S. Gerhard, S. Luscieti, M. Sanchez, L. Devireddy, J. Mol. Med. 90 (2012) 1209–1221.
[7] L.R. Devireddy, D.O. Hart, D.H. Goetz, M.R. Green, Cell 141 (2010) 1006–1017.
[8] K.N. Raymond, E.A. Dertz, S.S. Kim, Proc. Natl. Acad. Sci. U. S. A. 100 (2003) 3584–3588.
[9] J.H. Crosa, C.T. Walsh, Microbiol. Mol. Biol. Rev. 66 (2002) 223–249.
[10] K. Pantopoulos, S.K. Porwal, A. Tartakoff, L. Devireddy, Biochemistry 51 (2012) 5705–5724.
[11] L.R. Devireddy, C. Gazin, X.C. Zhu, M.R. Green, Cell 123 (2005) 1293–1305.
[12] D.R. Richardson, D.J.R. Lane, E.M. Becker, M.L.-H. Huang, M. Whitnall, Y.S. Rahmanto, A.D. Sheftel, P. Ponka, Proc. Natl. Acad. Sci. U. S. A. 107 (2010) 10775–10782.
[13] C. Correnti, V. Richardson, A.K. Sia, A.D. Bandaranayake, M. Ruiz, Y.S. Rahmanto, Z. Kovacevic, M.C. Clifton, M.A. Holmes, B.K. Kaiser, J. Barasch, K.N. Raymond, D.R. Richardson, R.K. Strong, PLoS ONE 7 (2012) 1–15.
[14] E. Furia, R. Porto, Ann. Chim. 92 (2002) 521–530.
[15] G. Biedermann, Sven. Kem. Tidskr. 76 (1964) 362.
[16] E. Furia, G. Sindona, J. Chem. Eng. Data 55 (2010) 2985–2989.
[17] L. Ciavatta, G. Nunziata, L.G. Sillén, Acta Chem. Scand. 23 (1969) 1637–1652.
[18] W. Forsling, S. Hietanen, L.G. Sillen, Acta Chem. Scand. 6 (1952) 901–909.
[19] A.S. Brown, J. Am. Chem. Soc. 56 (1934) 646–647.
[20] C.R. Evanko, D.A. Dzombak, J. Colloid Interface Sci. 214 (1999) 189–206.
[21] J.D. Chanley, E. Feageson, J. Am. Chem. Soc. 78 (1956) 2237–2241.
[22] P. Gans, A. Sabatini, A. Vacca, J. Chem. Soc. Dalton Trans. 6 (1985) 1195–1200.
[23] C.F. Baes, R.E. Mesmer, The Hydrolysis of Cations, A Wiley—Interscience Publication, New York, 1976.
[24] I. Grenthe, J. Fuger, R.J.M. Konigs, R.J. Lemire, A.B. Muller, C. Nguyen—Trung Cregu, H. Wanner, Chemical Thermodynamics of Uranium, in: Nuclear Energy Agency Data Bank (Ed.), 2004 (Issy—les–Moulineaux, France).
[25] D.V. Jahagirdar, J. Inorg. Nucl. Chem. 36 (1974) 2388–2390.
[26] A. Osol, L.J. Kleckner, J. Am. Pharm. Assoc. 41 (1952) 306–309.
[27] S.F.M. Ali, V.R. Rao, J. Inorg. Nucl. Chem. 37 (1975) 1041–1042.
[28] V.D. Khanolkar, D.V. Jahagirdar, D.D. Khanolkar, Indian J. Chem. 11 (1973) 286–287.
[29] A. Terauda, E.M. Shvarts, I. Vitola, I. Lange, G.V. Vladyko, E.I. Boreko, N.N. Sadovnikova, Latvijas PSR Zinatnu Akademijas Vestis, Kimijas Serija, 1985. 695–702.
[30] J. Kratsmar-Smogrovic, Acta Fac. Pharm. Bohemoslov. 10 (1965) 27–47.
[31] L. Sommer, Fresenius' Z. Anal. Chem. 171 (1960) 410–420.
[32] Y. Tanabe, K. Hata, Ann. Rept. Fac. Pharm., Kanazawa Univ. 6 (1956) 7–11.
[33] B. D. Zenner, C. S. Benedict, PCT Int. Appl. (1994) WO 9409084 A1 19940428.
[34] S. Paraskewas, L. Lapatsanis, Chemiker-Zeitung 103 (1979) 297–299.
[35] J.G. Wagner, J. Am. Pharm. Assoc. 42 (1953) 104–106.